Cerebral Cortex, November 2015;25: 4559–4571

doi: 10.1093/cercor/bhv096
Advance Access Publication Date: 20 May 2015
Original Article

ORIGINAL ARTICLE

A Novel Mechanism of Spine Damages in Stroke via DAPK1 and Tau

Lei Pei[1,4,†], Shan Wang[2,4,†], Huijuan Jin[2,4], Linlin Bi[2,4], Na Wei[2,4], Honglin Yan[2,4], Xin Yang[2,4], Chengye Yao[2,4], Mengmeng Xu[2,4], Shu Shu[2,4], Yu Guo[2,4], Huanhuan Yan[2,4], Jianhua Wu[2,4], Hao Li[2,4], Pei Pang[2,4], Tian Tian[2,4], Qing Tian[3,4], Ling-Qiang Zhu[3,4], You Shang[4,5], and Youming Lu[2,4,5]

[1]Department of Neurobiology, School of Basic Medicine, [2]Department of Physiology, School of Basic Medicine, [3]Department of Pathophysiology, School of Basic Medicine and, [4]The Institute for Brain Research (IBR), Collaborative Innovation Center for Brain Science, Huazhong University of Science and Technology, Wuhan, China and [5]Department of Critical Care Medicine, Institute of Anesthesia and Critical Care, Union Hospital, Wuhan, China

Address correspondence to You Shang and Youming Lu, the Institute for Brain Research, Collaborative Innovation Center for Brain Science, Huazhong University of Science and Technology, Wuhan 430030, China. Email: shang_you@126.com or lym@hust.edu.cn.

[†]Lei Pei and Shan Wang contributed equally to this work.

Abstract

Synaptic spine loss is one of the major preceding consequences of stroke damages, but its underlying molecular mechanisms remain unknown. Here, we report that a direct interaction of DAPK1 with Tau causes spine loss and subsequently neuronal death in a mouse model with stroke. We found that DAPK1 phosphorylates Tau protein at Ser262 (pS^{262}) in cortical neurons of stroke mice. Either genetic deletion of DAPK1 kinase domain (KD) in mice (DAPK1-$KD^{-/-}$) or blocking DAPK1-Tau interaction by systematic application of a membrane permeable peptide protects spine damages and improves neurological functions against stroke insults. Thus, disruption of DAPK1-Tau interaction is a promising strategy in clinical management of stroke.

Key words: DAPK1, dendritic spine, stroke, tau phosphorylation, therapeutics

Introduction

Stroke is caused by acute brain artery bursting or cerebral embolism, leading to neuronal death and sever dysfunction of synaptic transmission (Tu et al. 2010). Loss of synaptic spine has been considered the earliest event of cerebral ischemia and generally assumed to be associated with the subsequent brain damages (Hofmeijer and van Putten 2012). Thus, protection against synaptic loss is widely considered a promising strategy in stroke therapy.

Death-associated protein kinase 1 (DAPK1), a Ca^{2+}/CaM-dependent serine/threonine kinase, is originally identified by a functional cloning based on its involvement in interferon-γ-induced apoptosis (Bialik and Kimchi 2006). Our previous work demonstrated that following stroke, DAPK1 in the postsynaptic domain phosphorylated NMDA receptor NR2B at Serine-1303, eventually leading to neuronal death (Tu et al. 2010). Recently, we found that DAPK1 could also phosphorylate p53 at Serine-23

via direct binding of the DAPK1 death domain (DD) to the DNA-binding motif of p53 (p53DM) (Pei et al. 2014; Wang et al. 2014). Though a handful of DAPK1 substrates have been identified, downstream signaling of DAPK1 that specifically mediates early spine damage after ischemic injuries is yet to be characterized.

Tau protein colocalizes and co-immunoprecipitates with PSD95, a postsynaptic protein, and regulates the association of PSD-95 with NMDAR subunits, indicating the existence of endogenous Tau in dendritic spines probably participating in synaptic functions (Ittner et al. 2010). In addition, Tau abundantly contains high content of serine/threonine residuals and plays a crucial role in neurodegenerative diseases. There are 79 potential serine and threonine phosphorylation sites on the longest human Tau isoform. And phosphorylation of >30 of the phosphorylation sites has been reported (Morris et al. 2011). It is known that phosphorylation of these sites plays important roles in ischemic stroke-induced neuronal death (Lee et al. 2001; Zheng et al. 2010). However, the relative importance of individual phosphorylation site is still controversial.

In the present study, we demonstrated that DAPK1 directly phosphorylated Tau on Ser262, causing spine damage in the cortical neurons following stroke. We identified a binding domain of DAPK1 in the Tau microtubule repeat domains (R) with a sequence as ^{XX}IGSTENLK^{XX}. We synthesized a membrane-permeable blocking peptide (TAT-R1D) to disrupt DAPK1-Tau binding and Tau phosphorylation. We found that systematic administration of TAT-R1D, even 6 h after stroke, at a single dose of 2 mg/kg produced therapeutic effects against stroke damages.

Materials and Methods

Animals

Adult (90 ± 5 days old) male C57BL/6J mice were used and housed individually under standard conditions of temperature and humidity and a 12 h of light/dark cycle (lights on at 08:00) with free access to food and water. Adequate measures were taken to minimize pain or discomfort during surgeries. All the experiments were carried out in accordance with the Institutional Guidelines of the Animal Care and Use Committee (Huazhong University of Science and Technology).

Generation of DAPK1-KD Knockout Mice

To identify the specific impacts of DAPK1-kinase domain (DAPK1-KD) deletion in brain function, we generated a conditional mutant strain of mice with a selective deletion of DAPK1-KD in the brain (DAPK1-KD$^{-/-}$ mice) by crossing DAPK1-KD$^{loxp/loxp}$ transgenic mice (Tg1) and CaMK2α-creERT2 mice (Tg2). For details, see the Supplementary Material.

Focal Cerebral Ischemia Model

Focal cerebral ischemia was induced by intraluminal middle cerebral artery occlusion (MCAO). Briefly, a 7/0 surgical nylon monofilament with rounded tip was introduced into the left internal carotid through the external carotid stump and advanced 10–13 mm past the carotid bifurcation. Occlusion was confirmed when blood flow was reduced by at least 80% of the baseline. The filament was left in place for 60 min and then withdrawn. The sham-operated animals were treated identically, except that the middle cerebral artery was not occluded after the neck incision. Each mouse was anesthetized with 2% isoflurane and maintained with 1% isoflurane in an oxygen/air mixture by using a gas anesthesia mask in a stereotaxic frame (Stoelting). The rectal temperature was maintained during surgery at 37 ± 0.5°C with a homeothermic blanket (Harvard Apparatus).

TTC Staining

At indicated time point after ischemic reperfusion, brain was removed rapidly and frozen at –20°C for 5 min. Coronal slices (7 slices from each mouse) were made at 1 mm from the frontal tips, and sections were immersed in 2% TTC at 37°C for 20 min. The presence or absence of infarctions was determined by examining TTC-stained sections for the areas that did not stain with TTC.

AAV-eGFP Stereotaxic Injection and Dendritic Spine Analysis

Stereotactic injection of 2 μL of viral suspension containing 10E8 t.u. was at coordinates 1.94 mm posterior, 1.4 mm lateral and 2.2 mm ventral relative to bregma (Paxinos and Franklin, 2012). At indicated times after injection, the mice were anesthetized using pentobarbital (Nembutal) and perfused transcardially using 50 mL of ice-cold saline for 5 min. Brain were removed rapidly and fixed overnight in 4% paraformaldehyde for subsequent spine analysis on 40 μm free-floating coronal vibratome (VT1000S; Leica) sections. Immunofluorescent microscopy (LSM710, Zeiss) images were taken of cortical pyramidal neurons (73 cells with a total of 60 cm length of dendrites per group were analyzed) under 100 × oil lens. Images were coded and synaptic spines counted in software with Image Probes. All the spines were measured for spine densities analysis and expressed as spine/μm dendrite.

TUNEL Staining

At indicated time points after ischemia, animals were deeply anesthetized and transcardially perfused with 0.9% saline followed by ice-cold 4% paraformaldehyde in 0.1 M phosphate-buffered saline (PBS); the sections were dried overnight. A TUNEL staining kit (DeadEnd™ Fluorometric TUNEL system, Promega) was used to visualize cell death in 10-μm coronal frozen sections, as per kit instructions. Labeled sections were visualized with a confocal laser-scanning microscope (LSM710, Zeiss). All labeled cells within the reticule field (0.05 mm^2 at the magnification used) were counted using Image J throughout the depth of the section for 4 adjacent fields (beginning at a random starting position) of each section.

Double Immunofluorescent Staining

Animals were deeply anesthetized and transcardially perfused with saline, followed by 4% paraformaldehyde (in 0.01 M PBS, pH 7.4). Brain tissues were removed, post-fixed in 4% paraformaldehyde overnight, and then treated with 30% sucrose (in 0.1 M PB, pH 7.4) overnight till the tissue sink to the bottom. Cryosections (30 μm) were cut and stored at –20°C. Mounted brain sections were allowed to thaw at room temperature. Donkey or goat serum was used for blocking for 1 h. Next, the antibody to DAPK1 (rabbit, Cell Signaling Technology, #3008, 1:1000) and Tau (mouse,1:1000, MAB361, Millipore) or *p*S262 (mouse, 1:1000, SAB11111, Signalway Antibody) were incubated for 48 h. Fluorescein isothiocyanate (FITC)- and TRITC-conjugated second antibodies were then added and incubated for 1 h. The above-mentioned procedures were also used into primary cultured neurons (DIV 10) to identify the co-localizations of DAPK1 with Tau or with *p*S262. To visualize uptake of the peptide (Tat-R1D (IGSTENLK)-FITC) in the brain, standard immunostaining

procedures were performed on free-floating frozen sections (30 μm) with overnight incubation at 4°C with chicken anti-GFAP antibody (1:1000, Abcam,ab7260) or mouse anti-NeuN (1:1000, MAB377, Millipore) or mouse anti-Iba-1 antibody (1:1000, Abcam, ab5076), and then 2 h of incubation with anti-chicken Alexa594 or anti-mouse Alexa 594 antibodies, as well as 5 min of exposure to 4′,6-diamidin-2-phenylindol (DAPI, 1:10 000) as a counterstain. Slices were mounted on gelatin-coated glass slides, cover-slipped. The sections were examined with a laser-scanning confocal microscope (LSM 510, Carl Zeiss) using an omnichrome air-cooled helium/neon laser tuned to produce beams at 488 and 594 nm. Five randomly selected sections from the whole brain sections were used. All immunoreactive positive profiles in a section were outlined, creating an artificial overlay. Measuring the average optical density of double-labeled cells was conducted on confocal images randomly taken from 2 view fields from each section, and the measuring was performed using NIH Image J software.

Co-IP and GST Affinity Binding Assays

Ischemic core of the cortex samples were dissected in cold artificial cerebral spinal fluids (aCSF) and homogenized in 200 μl 0.32 M sucrose buffer (mM) (10 sucrose, 10 HEPES, pH 7.4) containing a "complete" protease inhibitor cocktail (Roche diagnostics). Samples were centrifuged (1000 × *g*, 10 min, 4°C) to yield the nuclear enriched pellet and the S1 fraction. The S1 fraction was centrifuged (12 000 × *g*, 20 min, 4°C) to obtain supernatant (S2; microsomes and cytosol) and pellet (P2; crude synaptosomal membranes) fractions. The S2 fraction was centrifuged (160 000 × *g*, 2 h, 4°C) to separate the cytosolic (supernatant) and microsomal (pellet) fractions. The P2 synaptosomal pellet was resuspended in 100 μl 4 mM HEPES buffer (mM) (4 HEPES, 1 EDTA, pH 7.4) and again centrifuged (12 000 × *g*, 20 min, 4°C). Resuspension and centrifugation was repeated. The resulting pellet was resuspended with buffer A (mM) (20 HEPES, 100 NaCl, 0.5% Triton, pH 7.2) and rotated slowly (15 min, 4°C), followed by centrifugation (12 000 × *g*, 20 min, 4°C). The supernatant (triton-soluble NP fraction) containing non-PSD membranes was retained. The pellet was resuspended in 120 μl buffer B (20 mM HEPES, 0.15 mM NaCl, 1% Triton-X, 1% deoxycholic acid, 1% SDS, 1 mM DTT, pH7.5), followed by gentle rotating (1 h, 4°C) and centrifugation (10 000 × *g*, 15 min, 4°C). The pellet was discarded and the supernatant (triton insoluble PSD fraction) retained. Microsomal, cytosolic, PSD and non-PSD samples were stored at –80°C until use. Protein concentration in the extracts was determined by Bradford assay (Bio-Rad). The extracts (500 μg protein) were incubated with nonspecific IgG (2 μg) or polyclonal rabbit anti-DAPK1 (2 μg; Cell Signaling Technology, #3008) or anti-Tau (2 μg, Millipore, MAB361) overnight at 4°C, followed by the addition of 40 μl of Protein G-Sepharose (Millipore, 16–266) for 3 h at 4°C. For the Co-IP experiments in HEK293 cells, the cells were lysed in IP buffer (mM) (20 Tris–HCl (pH 8.0), 100 NaCl, 1 EDTA, and 0.5% NP-40) containing protease inhibitor cocktail (Roche, 04693116001). After 20 min of incubation at 4°C with gentle vortex mixing, the cell lysates were centrifuged at 13 000 × *g* for 10 min at 4°C. Sample aliquots (500 μl) were precleared with 10 μl Protein A/G-agarose beads (11719394001, 11719386001, Roche) and incubated with 1 μg of antibody or control IgG overnight at 4°C, according to the manufacturer's recommendations. The precipitates were washed 4 times with lysis buffer and denatured with SDS sample buffer and separated by 12% SDS–PAGE. Proteins were transferred onto nitrocellulose membranes using a Bio-Rad mini-protein-III wet transfer unit overnight at 4°C. Transfer membranes were then incubated with blocking solution (5% nonfat dried milk dissolved in TBST buffer containing (mM): 10 Tris–HCl, 150 NaCl, and 0.1% Tween-20) for 1 h at room temperature, washed 3 times, and incubated with primary antibody against anti-DAPK1 (Cell Signaling Technology, #3008, 1:1000) or anti-Tau (Millipore, MAB361, 1:1000) for 1 h at room temperature. Membranes were washed 3 times with TBST buffer and incubated with the appropriate secondary antibodies for 1 h followed by washing 4 times. Signal detection was performed with an enhanced chemiluminescence kit (Amersham Biosciences). The lanes marked "input" were loaded with 10% of the starting material used for immunoprecipitation.

To determine the binding domain of DAPK1 with Tau protein, the DAPK1 deletion mutants (Flag-DAPK1$^{\Delta DD}$, Flag-DAPK1$^{\Delta KD}$, Flag-DAPK1^{K42A} and Flag-DAPK1$^{\Delta CaM}$) were generated from full-length cDNA mouse DAPK1$^{1-1431}$. Purified Flag fusion proteins were separated using SDS–PAGE and transferred onto a nitrocellulose membrane, which was washed with distilled water and blocked with TBST for 1 h at room temperature. The membrane was then incubated with affinity binding buffer containing 50 mM Tris–HCl (pH 7.5), 200 mM NaCl, 12 mM-mercaptoethanol, 1.0% polyethylene glycol, 10 μg/ml protease inhibitors, and 500 μg/ml purified GFP-tagged Tau40 for 1 h at room temperature and washed 4 times for 5 min with affinity binding buffer. Bound DAPK1 and Tau40 was detected with anti-Flag (1:2000, Invitrogen) and anti-GFP (1:1000, Invitrogen), respectively.

Recombinant DNA Construction

The truncated DAPK1 constructs, including DAPK1$^{\Delta KD}$ (residues 288–1430), DAPK1$^{\Delta CaM}$, DAPK1$^{\Delta DD}$ (residues 1–1398), and DAPK1^{K42A} mutants, were received as a gift from Prof. R-H Chen (Institute of Biological Chemistry, Academia Sinica). The vectors were re-cloned into the rAVE construct through ApaI/KpnI (GenDetect).

cDNA encoding Tau40 in pRK5 was used as the template for PCR amplification. The PCR products were digested using *SalI* and *Cla1*. The resulting fragment was ligated to an *SalI*-digested rAVE-eGFP vector (GenDetect, Ltd.) to generate rAVE-Tau40-eGFP under the control of a CAG enhancer and was terminated using the polyadenylation signal in the 3′ long terminal repeat. Phospho-deficient (substitution of serine at position 262 to alanine, S262A) construct was created by site-directed mutagenesis using the QuikChange Kit (Agilent Technologies) according to the supplier's manual and verified by sequencing analysis. Tau-S262A and Tau-WT (wild type) were subcloned into the rAVE-eGFP vector (GenDetect, Ltd.). rAVE-Tau40-eGFP or rAVE-Tau-S262A-eGFP was co-transfected with the AAV helper 1/2 into HEK293 cells to generate high titers (9×10^{12} genomic particles/ml) of rAAV1/2 infectious particles.

Phosphorylation Site Analysis by Mass Spectrometry

Phosphorylation can occur at a serine (S), threonine (T) or tyrosine (Y) residue. We identified phosphorylated residues in the Tau sequences using phosphorylated residue prediction tool, GPS2.1 (Xue et al. 2008). The prediction threshold value for GPS2.1 was set to be "high." To further confirm the predicted phosphorylation sites, purified DAPK1-precipitated Tau protein samples were separated by SDS–PAGE gel. Corresponding areas of phosphorylated Tau (*p*Tau) (40–70 kDa) were cut out from the coomassie blue stained SDS–PAGEs. Gel pieces underwent in-gel digestion and were subjected to a nanoLC-ESI-Iontrap mass spectrometer (BrukerDaltonik GmbH). Each spectrum was internally calibrated with mass signals of trypsin autolysisions to reach a typical mass measurement accuracy of ±10 ppm. Raw data were searched in the SWISS-PROT database.

Primary Neuron Culture and Plasmid Transfection

Cerebral cortex was isolated from the E20 wild-type mice or DAPK1-KD$^{-/-}$ mice, as we described before (Tu et al. 2010; Yang et al. 2012). Cells were dissociated and purified using papain dissociation kit (Worthington Biochemical Corporation) platted with the densities of 100–150 cells/mm^2 on 19-mm coverslips coated with 30 μg/ml poly-D-lysine and 2 μg/ml laminin. Cells were placed in fresh serum-free Neurobasal Medium (21 103, GIBCO) plus 2% B27 and fed every 4 days with fresh media. The cultures were immunostained for β-tubulin III (Tuj1), a neuronal marker to confirm that these cultures were >85% neurons. On Day 9 (DIV 9), DAPK1 or DAPK1-KD$^{-/-}$ was co-expressed with a wild-type Tau (Tau-WT) or Tau-S262A mutant (S262A) in HEK293 cells using the respective rAAV1/2-virus particles, as indicated.

Electrophysiology

Whole-cell patch-clamp recordings were performed in voltage clamp mode using Axopatch 200B amplifier (Axon Instruments, Inc.), digitized at 10 kHz and filtered at 2 kHz. Data were acquired and analyzed using Clampfit 10.0 software (Axon Instruments, Inc.). Whole-cell recording pipettes (3–5 MΩ) were filled with a solution containing (in mM): 120 CH_4SO_3, 20 $CaCl_2$, 4 NaCl, 10 HEPES, 0.05 EGTA, 4 Mg_2ATP, 0.2 Na_3GTP, 5 QX314 and ~290 mOsm. The bath solution contained (in mM): 124.0 NaCl, 3.0 KCl, 26.0 $NaHCO_3$, 1.2 $MgCl_2$•$6H_2O$, 1.25 NaH_2PO_4•$2H_2O$, 10.0 $C_6H_{12}O_6$, 2.0 $CaCl_2$ (pH 7.4), ~305 mOsm. Miniature AMPAR-dependent EPSCs were isolated by including D-APV (50 μM), bicuculine (10 μM), and 1 μM tetrodotoxin in the bath solution. All recordings were performed at a holding potential of −70 mV at room temperature. mEPSCs were identified using a template with a threshold of −6 pA (2.5 × SD of the noise) and were individually proofread for accuracy. To plot summary graphs, the average frequency from the eGFP control cells from each culture preparation was normalized. Individual cells from all 4 conditions were then compared with this normalized average.

Magnetic Resonance Imaging

Animals were anesthetized with isoflurane 1.5–2% and kept at 37°C, and an MR compatible respiration sensor was used to control the animals. All the magnetic resonance imaging (MRI) experiments were performed on a BIOSPEC BMT 47/40 (Bruker) spectrometer operating a 4.7T, equipped with an 11.2-cm actively shielded gradient system, capable of 200 mT/m gradient strength and 80 μs of rise time. A 7-cm bird cage radiofrequency coil was used for transmission and reception. T2-Weighted Imaging (T2WI) were acquired using a rapid acquisition with relaxation enhancement (RARE) technique, with a repetition time (TR) = 1650 s, RARE factor = 16, and inter echo interval = 10 ms, resulting in an effective echo time (TE) = 80 ms, the field of view (FOV) = 4 × 4 × 4 cm^3. The acquired matrix size was 128 × 128 × 64. These data were zero-filled to obtain a reconstructed matrix size of 128 × 128 × 128.

Fluoro-Jade C Staining

The brain tissue slides were immersed for 3 min in 100% ethanol, for 1 min in 70% ethanol, and for 1 min in distilled water and then incubated in a solution containing 0.01% Fluoro-Jade C (Millipore) and 0.1% acetic acid (1:10) for 30 min on a shaker. After three 10-min washes, the slides were cover-slipped and imaged with a laser-scanning confocal microscope (LSM 510, Carl Zeiss). The number of FJ positive (FJ$^+$) cells in each group was counted.

Golgi Staining and Synaptic Spine Analysis

Brains were removed from mice and immediately immersed in Solution A and B for 2 weeks at room temperature and transferred into Solution C for 24 h at 4°C, as instructed on the manufacture's experimental methods (FD rapid Golgi Stain kit, FD NeuroTechnologies). The brains were sliced using a Vibratome (VT1000S; Leica) at a thickness of 100 μm. Bright-field microscopy (Axio Observer; Zeiss) images were taken of cortex pyramidal neurons (50 cells with a total of 60 cm length of dendrites per group were analyzed). Images were coded and synaptic spines counted in software with Image Pro plus 6.0. All the spines were counted, and spine densities were expressed as spine/μm dendrite.

Administration of Peptides

The mice underwent a 60 min MCAO were injected (i.v.) with vehicle (saline) or TAT-R1D or TAT-s-R1D at a single dose of 0.5, 1, 2, 5, or 10 mg/kg body weight. In another group, 3, 6, or 9 h after MCAO, mice were injected with vehicle or TAT-R1D or TAT-s-R1D (2 mg/kg body weight, i.v.). The peptides were numbered and the experimenters were unaware of which one was applied in all experiments.

Neurological Score

Neurological performance was scored daily using modified 7-point neurological scales (Tu et al. 2010); 0, no observable neurological deficits; 1, flexion of the contralateral torso; 2, circling to the ipsilateral side but normal posture at rest; 3, circling to the ipsilateral side; 4, rolling to the ipsilateral side; 5, leaning to the ipsilateral side at rest; 6, longitudinal spinning; and 7, no spontaneous motor activity/death. Score were ranked from 0 to 7 at an interval of 1.0. Neurological performance was always assessed by the blinded independent investigators.

Rotarod Treadmill Test

Motor coordination of the animals after operation and treatment was measured using a rotarod treadmill for mice (Ugo Basile), under the accelerating rotor mode (10 speeds from 4 to 40 rpm for 5 min). The interval from when the animal mounted the rod to when it fell off was recorded as the retention time, and the population of mice that walked for 300 s on the accelerating rotating rod was recorded as the walking survivor (Chen et al. 2012). The animals were trained for 2 days, 3 trials per day, before surgery, and the mean duration on the rod was recorded to obtain stable baseline values. Performance on the rotarod test was measured 3 times a day in the following 4 weeks after ischemic insult and peptide administration.

Data Analysis

All variance values in the text and figure legends are represented as mean ± SEM. Western blot results, spine analysis data, infarct volumes, TUNEL or FJ staining positive cells, Neurological scores, and electrophysiology data were analyzed using the ANOVA with the Student–Newman–Keuls (SNK) tests. The data of behavioral studies were analyzed by two-way repeated-measures ANOVA with Bonferroni comparisons. Statistical analyses were performed using SPSS 13.0 (IBM) and Sigmaplot 12.0. Statistically significant differences were defined as $P < 0.05$.

Results

Spine Damage Precedes to Apoptosis in Cerebral Ischemia

Dendritic spine density in the cortical neurons was analyzed in the frontal cortex of 2, 6, 12, and 24 h reperfusion after 1 h of MCAO by confocal imaging in brain tissue with AAV-eGFP infection 15 days before MCAO surgery (Fig. 1A). In total, 1560 spines were counted on 30 dendrites per group. Hereby, we detected significant decreases in dendritic spine density from 2 h to 24 h after MCAO (Fig. 1B,C). Consistently, the synaptic related proteins, postsynaptic density protein 95 (PSD95), AMPA receptor subunit GluR1 (GluA1), and Synapsin 1, were dramatically decreased 2 h after MCAO in the ischemic area (Fig. 1D,E). Simultaneously, the TUNEL-labeled (TUNEL$^+$) apoptotic cells in the same brain area were examined at 2, 6, 12, and 24 h of reperfusion after 1 h MCAO. We observed notable increases of TUNEL$^+$ cells from 6 h to 24 h after MCAO (Fig. 1F,G). In parallel, the protein levels of cleaved caspase 3 (Casp.3) were significantly increased 12 h after ischemic injury (Fig. 1H,I). Taken the above results together, we found the spine damage was prior to apoptosis in cerebral ischemia.

DAPK1 Interacts with Tau via its KD

To test whether DAPK1-Tau interaction mediates spine damage, we first examined whether DAPK1 interacts with Tau in ischemic brain tissue and primary cultured neurons under oxygen glucose

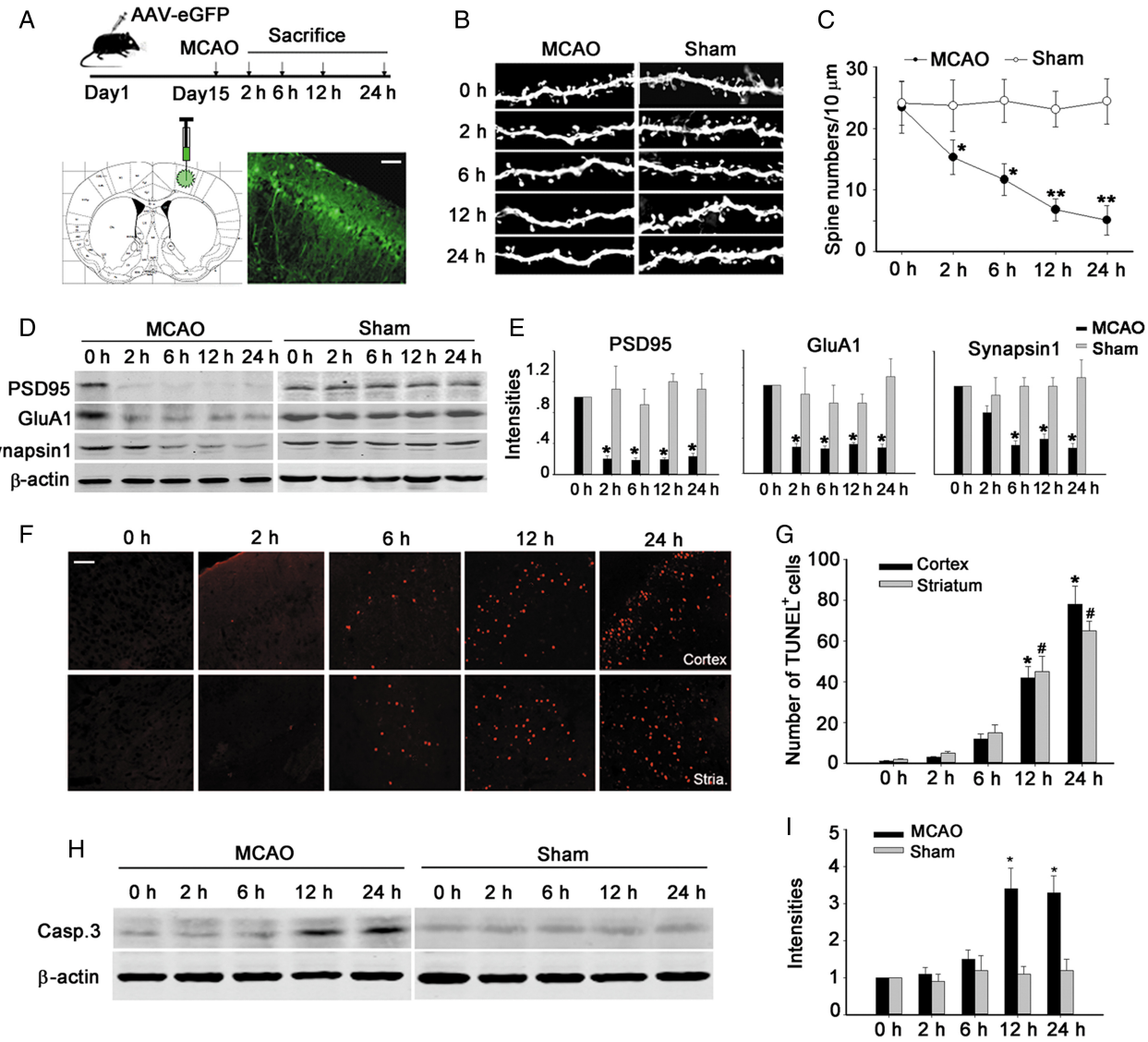

Figure 1. Spine damage is prior to apoptosis in stroke. (*A*) Experimental schedule in the upper panel; illustration in the lower panel shows representative images of the AAV-eGFP-infected cortex area in the mouse brain. Scale bar: 100 μm. (*B*) High-resolution images of dendritic spines in the vicinity (distance < 30 μm) of ischemic core area in the cortex. (*C*) Quantification of the dendritic spine density in the cortex at indicated time points after MCAO or sham treatment ($n = 6$ mice). *$P < 0.05$; **$P < 0.01$ vs. sham. (*D*) Immunoblots for PSD95, GluA1, and Synapsin 1 after 2, 6, 12, and 24 h of reperfusion. (*E*) Quantification of the protein levels, band intensities at 2, 6, 12, and 24 h were normalized to 0 h ($n = 5$ mice). *$P < 0.05$ vs. sham. (*F*) Representative images of the ischemic cortex and striatum with TUNEL staining after 2, 6, 12, and 24 h of reperfusion. Scale bar: 100 μm. (*G*) Quantification of the numbers of TUNEL-positive cells ($n = 6$ mice per time point). *$P < 0.05$ (cortex), #$P < 0.05$ (striatum) vs. 0 h, respectively. (*H*) Immunoblots for cleaved caspase 3 (Casp. 3) after 2, 6, 12, and 24 h of reperfusion. (*I*) Quantification of the protein levels, band intensities at 2, 6, 12, and 24 h were normalized to 0 h ($n = 5$ mice). *$P < 0.05$ vs. Sham. Data are presented as mean ± SEM.

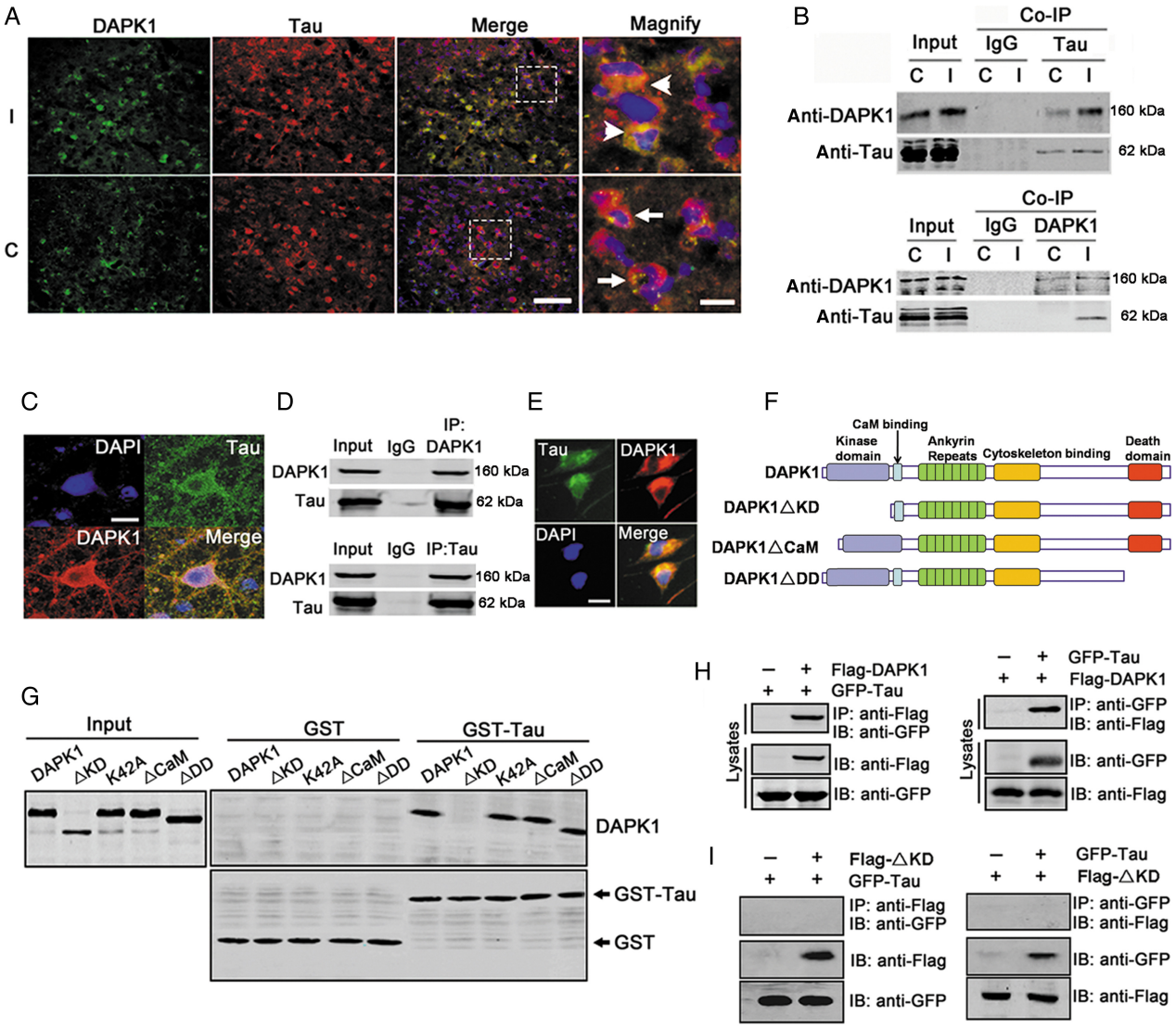

Figure 2. A direct binding of DAPK1-KD with Tau. (*A*) Representative images of the ischemic cortex after 24 h of reperfusion double stained with DAPK1 (green) and Tau (red) antibodies. Hoechst staining (blue) was used to label the nucleus. Scale bar: 100 μm in the merged pictures or 20 μm in the magnified pictures. (*B*) Co-IP of 500 μg of proteins from ischemic mouse cerebral cortex with nonspecific IgG (IgG), anti-DAPK1, or anti-Tau, as indicated. Input: 20 μg of protein of the extracts without IP was loaded (C, Contralateral; I, Ipsilateral). (*C*) Co-localization of DAPK1 and Tau in the OGD-treated primary cultured cortex neurons (DIV 12). Scale bar, 20 μm. (*D*) Co-IP of DAPK1 and Tau in the primary cultured cortex neurons (DIV12). The lysates were immunoprecipitated with anti-DAPK1 or anti-Tau and analyzed by immunoblotting using anti-DAPK1 or anti-Tau antibody. (*E*) Co-localization of DAPK1 (red) and Tau (green) in the cytoplasm of DAPK1 and Tau co-transfected HEK293T cells; the nuclei were stained with DAPI. Scale bar, 10 μm. (*F*) Schematic shows the constructs of full length DAPK1, mutant plasmids of DAPK1 (DAPK1ΔKD, DAPK1ΔCaM, and DAPK1ΔDD). (*G*) Tau binding to the KD of DAPK1. HEK293T cells expressing DAPK1 or its mutants were subjected to GST pull-down assays. (*H*) Co-IP of DAPK1 and Tau in Flag-tagged DAPK1 and GFP-tagged Tau co-transfected HEK293T cells. The lysates were immunoprecipitated with anti-Flag or anti-GFP and analyzed by immunoblotting using anti-Flag or anti-GFP antibody. (*I*) HEK293T cells were transfected with GFP-tagged Tau, and Flag-tagged DAPK1-KD deletion mutant (Flag-ΔKD) were immunoprecipitated from lysates with anti-Flag and immunoblotted with anti-Flag and anti-GFP antibodies.

deprivation (OGD). By double immunofluorescent staining and co-immunoprecipitation, we found that endogenous DAPK1 and Tau formed a complex in ischemic stroke (Fig. 2*A*–*D*). Though the expression of DAPK1 and Tau was not changed after ischemia (Supplementary Fig. S1*A*,*B*), the activity of DAPK1, which is reflected by phosphorylation of Myosin Light Chain (*p*MLC, a substrate of DAPK1 to reflect DAPK1 catalytic activity), was substantially increased 2 and 24 h after stroke onset (Supplementary Fig. S1*C*).

To learn how DAPK1 associates with Tau, we co-transfected GFP-tagged Tau (GFP-Tau) with Flag-tagged DAPK1 (Flag-DAPK1) into HEK293T cell. GFP-Tau might combine with Flag-DAPK1 (Fig. 2*E*) and form stable complexes. To identify the domain(s) in-DAPK1 necessary for the interaction, we generated different DAPK1 mutants (Fig. 2*F* and Supplementary Fig. S2*A*,*B*). GST pull-down experiments revealed that GST-Tau, but not control GST, bound to Flag-DAPK1, its constitutively active form Flag-DAPK1$^{\Delta CaM}$, inactive form Flag-DAPK1^{K42A} and DD deletion form Flag-DAPK1$^{\Delta DD}$, except DAPK1 KD deletion form Flag-DAPK1$^{\Delta KD}$ (Fig. 2*G*). In addition, as shown by co-immunoprecipitation, all DAPK1 mutants could bind to Tau, except the DAPK1 KD deletion mutant (Flag-DAPK1$^{\Delta KD}$) (Fig. 2*H*,*I* and Supplementary Fig. S2*C*–*E*), suggesting that the KD is necessary for DAPK1 binding to Tau.

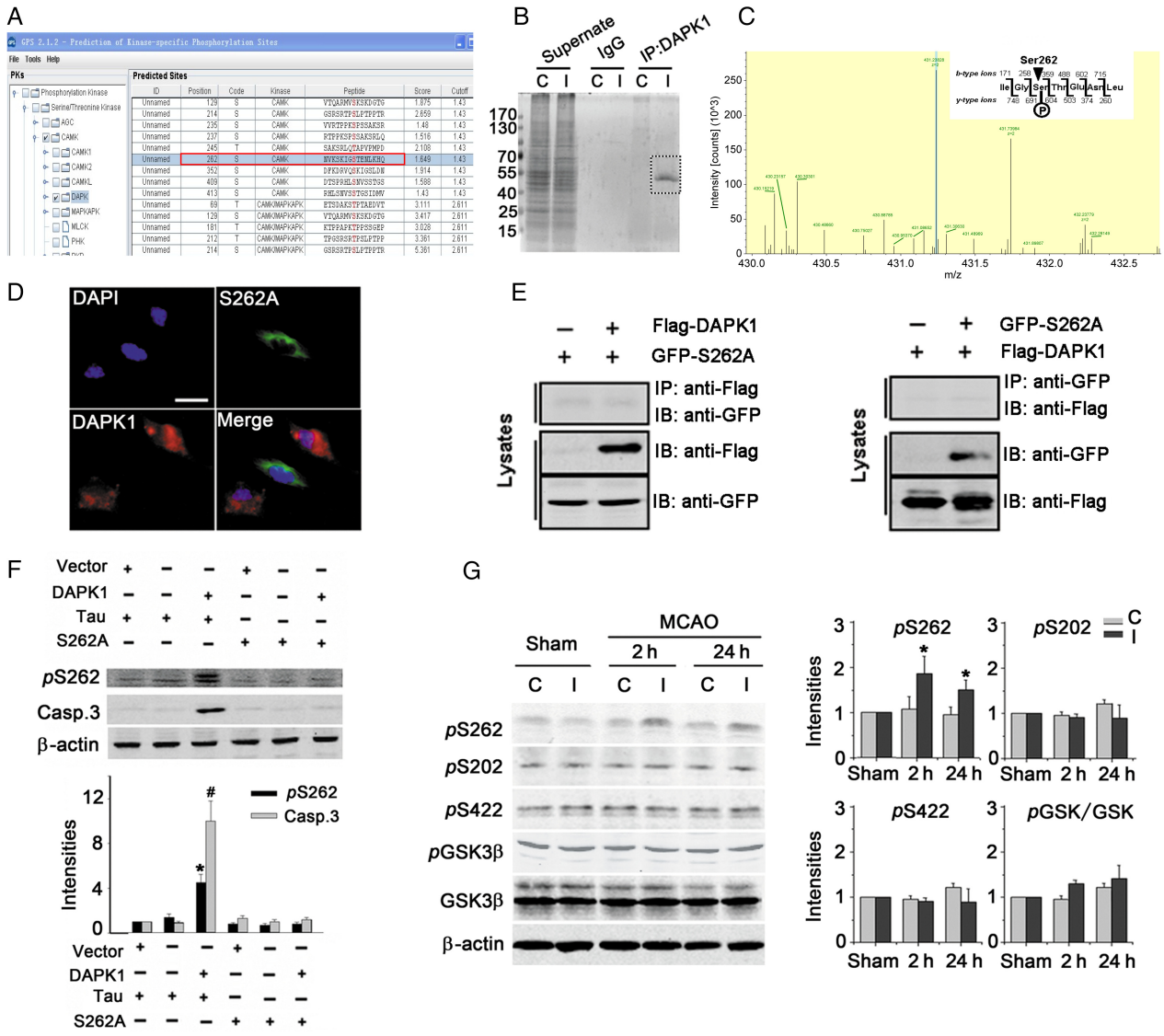

Figure 3. DAPK1 phosphorylates Tau on Ser262 in vitro and in vivo. (*A*) Prediction of Tau phosphorylation sites by DAPK1 via GPS 2.1 software. (*B*) The immunoprecipitates with supernatant, nonspecific IgG, or an antibody against DAPK1 in the extracts (5 μg proteins) from the mice cortex 24 h after reperfusion were stained with Coomassie blue (C, contralateral; I, ipsilateral). (*C*) Base peak chromatogram of mass spectrum from trypsin-digested products of the corresponding SDS gel with band ranging from 40–70 KD (box area in B). (*D*) Immunofluorescent double-staining of DAPK1 (red) and S262A (green) in co-transfected HEK293T cells; the nuclei were stained with DAPI. Scale bar: 10 μm. (*E*) Co-IP of DAPK1 and S262A in Flag-DAPK1 and GFP-S262A co-transfected HEK293T cells. The lysates were immunoprecipitated with anti-Flag or anti-GFP and analyzed by immunoblotting using anti-Flag or anti-GFP antibody. (*F*) Immunoblots of the extracts from DAPK1 and Tau or DAPK1 and S262A co-transfected HEK293T cells with anti-*p*S262 and anti-Casp.3 antibodies. Lower panel shows the quantification of the protein levels; band intensities were normalized to Vector and Tau co-transfected group ($n = 3$). *$P < 0.05$ (*p*S262) or #$P < 0.05$ (Casp.3) vs. Vector and Tau co-transfected group. (*G*) Immunoblots of the extracts from the ischemic mice cortex 2 and 24 h after reperfusion incubated with *p*S262, *p*S202, *p*S422, *p*GSK3β, and GSK3β antibodies (C, contralateral; I, ipsilateral). Right panel shows the quantification of the protein levels; band intensities were normalized to sham group ($n = 3$). *$P < 0.05$ vs. sham. Data are presented as mean ± SEM.

DAPK1 Phosphorylates Tau on Ser262 in Stroke

Given DAPK1 associated with Tau, a central question is whether DAPK1 phosphorylates Tau in vitro and in vivo. To determine whether Tau is a substrate of DAPK1 we directly assessed Tau phosphorylation site by the prediction software GPS 2.1 and nano-LC-ESI-MS/MS analysis. GPS 2.1 analysis suggested Ser262 of Human tau isoform (NCBI Reference Sequence: NP_005901.2) as a potential phosphorylation site for DAPK1 (Fig. 3A). Mass spectrum also demonstrated the Ser262 of Human tau isoform within the peptide *IGSTENLK* by DAPK1 after ischemic injury (Fig. 3B,C; Supplementary Fig. S2A, Supplementary Table S1 and S2). Blast results from the NCBI protein database revealed that the peptide *IGSTENLK* is highly conserved among different mammalian species (Supplementary Fig. S2B). No other Tau phosphorylation site than Ser-262 was identified in the Mass Spectrum assay (Supplementary Table S3).

To further validate Human Tau Ser262 as the phosphorylation site for DAPK1 in vitro, we generated a mutant form of Tau in which the phosphorylation site Serine 262 was mutated to Alanine 262 (S262A) and co-expressed DAPK1 in the HEK293 cells with S262A. Immunocytochemistry results demonstrated DAPK1 did not co-localize with S262A (Fig. 3D). In addition, co-immunoprecipitation experiments showed that DAPK1 did not

interact with S262A (Fig. 3E). Western blottings also showed that the expression of *p*S262 was dramatically increased in parallel with cleaved caspase 3 in HEK293 cells transfected with DAPK1 and Tau-WT, but not DAPK1 and S262A (Fig. 3F).

To further investigate phosphorylation of Tau on Ser-262 after ischemia in vivo, we next subjected C57BL/6 mice with MCAO for 60 min and examined Tau phosphorylation. Western blotting results showed that *p*S262, but not previously reported *p*S202 or *p*S422, was detected. It is known that glycogen synthase kinase 3β (GSK3β) is a key regulatory kinase of Tau. Unexpectedly, neither GSK3β nor its activated form, phosphorylated GSK3β (*p*GSK3β), is significantly altered within 24 h after MCAO operation (Fig. 3G). These results indicate that DAPK1 phosphorylates Tau on Ser262 in cerebral ischemic stroke.

Phosphorylation of Tau on Ser262 Induces Spine Damage

Next, we co-transfected Tau-WT with DAPK1, S262A with DAPK1 into cultured primary cortical neurons or transfected Tau-WT into DAPK1-KD$^{-/-}$ cortical neurons from DAPK1-KD$^{-/-}$ mice to test whether Tau phosphorylation at Ser262 by DAPK1-KD mediates spine damage and neuronal apoptosis. Tau or S262A was fused with eGFP for visualization. DAPK1 and Tau-WT were co-transfected in cultured neurons at 9 days in vitro (DIV 9)

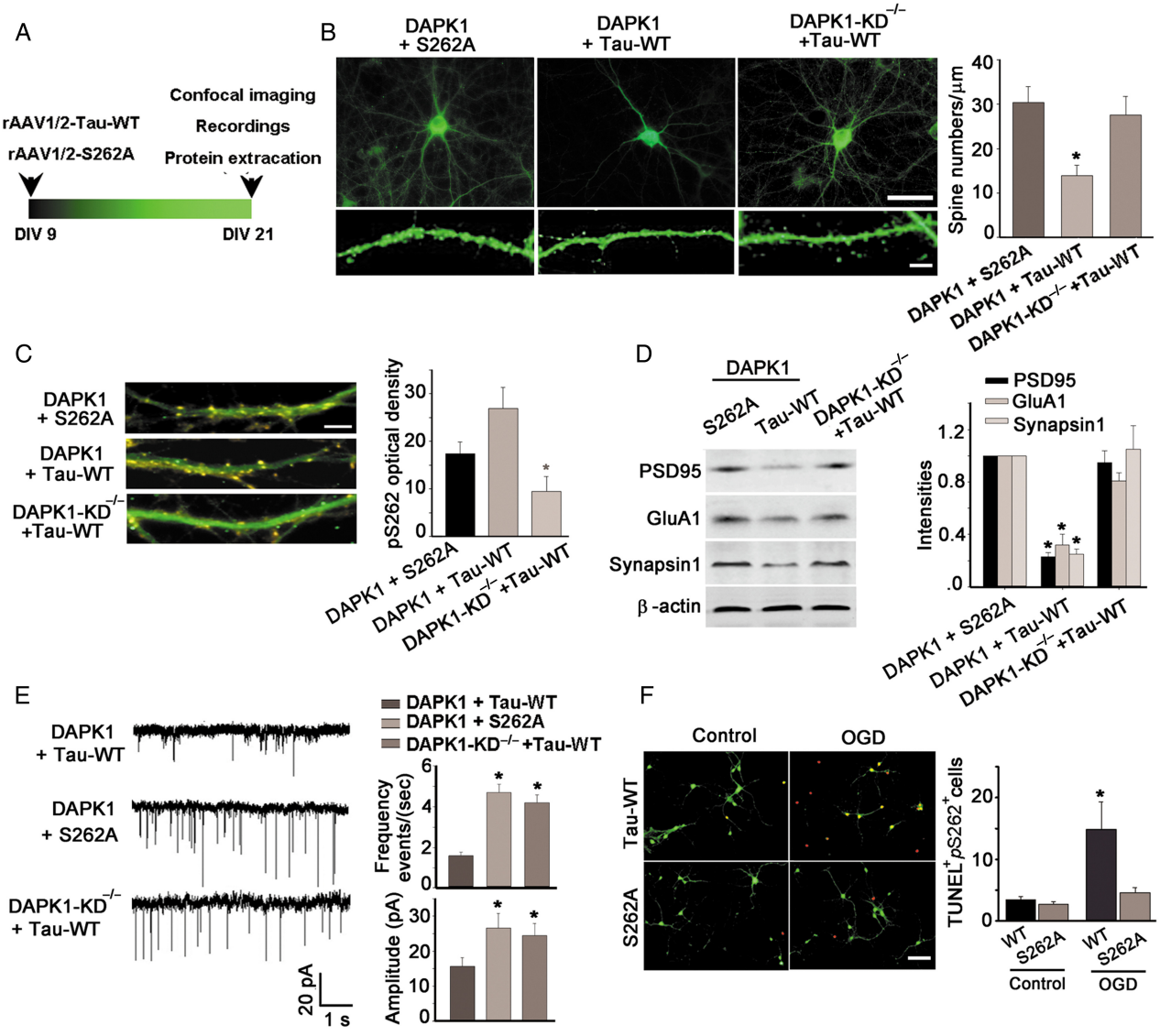

Figure 4. Phosphorylation of Tau on Ser262 induces spine damage. (*A*) Illustration shows the experimental procedure. (*B*) Confocal images of AAV-infected primary cultured cortex neurons (DIV 21) co-expressing DAPK1 with S262A, or DAPK1 with Tau-WT and DAPK1-KD$^{-/-}$ neurons (DIV 21) expressing Tau-WT. Bar graph shows the quantification of total spines in neurons among different groups. Scale bar: 50 μm in the upper panel, 10 μm in the lower panel. (*C*) DAPK1 and *p*S262 double-labeled spines (yellow) from DAPK1 and S262A, DAPK1 and Tau-WT co-expressing neurons or Tau-WT expressing DAPK1-KD$^{-/-}$ neurons. Bar graph shows the quantification of the optical densities of *p*S262 on the spines ($n = 11$ cultures). Scale bar: 10 μm. $^*P < 0.05$ vs. DAPK1 + Tau-WT group. (*D*) Immunoblots experiments show the protein levels of PSD-95, GluA1, and Synapsin1 among different groups. Data quantification is shown in the left bar graph. (*E*) Sample traces of mEPSCs recorded at −70 mV in neurons co-transfected with DAPK1 and Tau-WT, or DAPK1 and S262A, or in DAPK1-KD$^{-/-}$ neurons transfected with Tau-WT. The summary graphs from 8 culture sets of normalized mEPSCs frequency and amplitude are shown beside the traces. $^*P < 0.05$ vs. DAPK1+Tau-WT group. (*F*) OGD-treated S262A or Tau-WT-transfected primary cultured cortical neurons double-labeled with TUNEL (red) and anti-*p*S262 antibody (green). Bar graph shows the quantification of the TUNEL$^+$/*p*S262$^+$ cells ($n = 5$ mice). Scale bar: 50 μm. $^*P < 0.05$ vs. S262A with OGD treatment. Data are presented as mean ± SEM.

(Fig. 4A). We found that 12 days after transfection, there was a significant decrease in spine density (Fig. 4B), an increase in synaptic *p*S262 (Fig. 4C), and a reduction in synaptic proteins including PSD95, GluA1, and Synapsin 1 (Fig. 4D). Consistently, we found a significant decline in both amplitude and frequency of AMPAR-mediated miniature excitatory postsynaptic current (mEPSC) (Fig. 4E). On the contrary, co-transfection of DAPK1 with S262A or transfection of Tau-WT in DAPK1-KD$^{-/-}$ neurons decreased *p*S262 level and alleviated spine loss (Fig. 4B–E).

To further define the effect of *p*S262 on neuronal apoptosis after ischemic insults in vitro, we treated the primary cultured neurons with OGD. We found that the TUNEL^{+}/*p*S262^{+} cells were significantly decreased 60 min after OGD treatment in S262A-transfected neurons compared with Tau-WT transfected neurons (Fig. 4F). Taken together, these results suggest that Tau is probably a major mediator of DAPK1 toxicity on dendritic spines and synaptic functions, which is largely dependent on phosphorylation of Ser262.

Genetic Deletion of DAPK1-KD Protects against Stroke Damage

To confirm the role of DAPK1-KD on spine damage and stroke injuries in vivo, we generated a conditional mutant strain of mice with a selective deletion of DAPK1-KD in the brain (DAPK1-KD$^{-/-}$ mice) by crossing CaMK2α-creERT2 and DAPK1-KD-Floxed transgenic mice (DAPK1-KD$^{loxp/loxp}$ mice) (Supplementary Fig. S4A). Deletion of KD induced 80% reduction in DAPK1-KD mRNA (Supplementary Fig. S4B) and >90% decrease of DAPK1 N terminal protein (Supplementary Fig. S4C). Furthermore, conditional knockout KD did not influence the animals' phenotype, such as body weight gain (Supplementary Fig. S4D,E), cerebral blood vessels and blood flow (Supplementary Fig. S4F), brain structure (Supplementary Fig. S4G), and anxiety-like behavior (Supplementary Fig. S4H). These results confirmed the successful deletion of KD in the brain, and this deletion exerted no significant phenotypic changes on mice.

Next, we subjected the DAPK1-KD$^{-/-}$, and DAPK1-KD$^{loxp/loxp}$ mice with MCAO for 60 min and performed MRI studies 24 h after reperfusion. Magnetic resonance imaging revealed a marked reduction of infarction area (13.6 ± 4.2 mm^3) when compared with the control DAPK1-KD$^{loxp/loxp}$ mice (47.8 ± 5.1 mm^3) (Fig. 5A). Furthermore, immunoblotting of infarct brain tissue from the DAPK1-KD$^{-/-}$ mice showed lesser *p*S262, more PSD95, GluA1, and Synapsin1 24 h after ischemia than the DAPK1-KD$^{loxp/loxp}$ mice (Fig. 5B). Three days after reperfusion, frozen brain sections were prepared and stained with Fluoro-Jade C (FJ) to detect neuronal death, and an unbiased stereological analysis was adopted to measure the FJ-labeled (FJ^{+}) area in the ischemic brain. Much less neuronal death was detected in DAPK1-KD$^{-/-}$ mice compared with DAPK1-KD$^{loxp/loxp}$ mice (Fig. 5C). The reduction of brain infarction area was associated with alleviated spine loss (Fig. 5D), improved neurological scores and motor coordination in DAPK1-KD$^{-/-}$ mice (Fig. 5E,F). These results further confirmed the above-mentioned conclusion that phosphorylation of Tau on Ser262 by DAPK1-KD induces spine damage after ischemia.

TAT-R1D Produces the Therapeutic Effects against Stroke Damage

Given that we have confirmed the interaction of DAPK1-KD with the microtubule repeat binding domain 1 of Tau (R1D) consisting of amino acids IGSTENLK, we hope to further explore the significance of the association. To this end, we generated a membrane-permeable peptide by fusing the peptide IGSTENLK to the transduction domain of the HIV TAT protein, named TAT-R1D. The HPLC graph and parameters of the purified peptide IGSTENLK are shown in Supplementary Figure S5A. Fluorescein isothiocyanate was fused to the terminal of TAT-R1D to visualize neuronal uptake of the peptide. We operated adult male mice with MCAO for 60 min followed by reperfusion. Three hours later, animals were intravenously (i.v.) administered with a single dose of 0.5, 1, 2, 5, or 10 mg/kg TAT-R1D, scrambled control peptide (TAT-s-R1D) or vehicle control (saline) (Fig. 6A, upper panel). Our data showed that intravenous injection-induced uptake of TAT-R1D into neuronal cells, but not microglia or astrocytes (Supplementary Fig. S5B). At a dose of 2 mg/kg (i.v.), TAT-R1D effectively disrupted the DAPK1-Tau association in brain tissues (Fig. 6B). To evaluate the intervention time window, we administered mice with TAT-R1D (2 mg/kg, i.v.) at 3 indicated time points (3, 6, and 9 h after reperfusion) (Fig. 6A, lower panel). Three and six hours after reperfusion, TAT-R1D was effective in dissociating DAPK1-Tau interaction (Fig. 6C). These results indicate that the 2 mg/kg (i.v.) may be used as an effective dose and 6 h after reperfusion may be taken for proper treatment time window.

To investigate the protective effects of TAT-R1D against spine damage after stroke, we examined the levels of *p*S262 and synaptic-related proteins. After treatment with TAT-R1D (2 mg/kg body weight, i.v.) 6 h after MCAO, immunoblotting of extraction of cortex tissue 24 h after MCAO showed inhibition in *p*S262 expression (Fig. 6D), prevention of the loss of both postsynaptic (PSD-95 and GluA1) and presynaptic proteins (Synapsin1) (Fig. 6E). Consistently, the reduction in both amplitude and frequency of AMPAR-mediated mEPSC after MCAO was rescued by TAT-R1D application (Fig. 6F). These results demonstrate that TAT-R1D is effective and efficient in blocking ischemia-induced spine damage.

To further confirm whether TAT-R1D might be used as a potential neuroprotective agent in stroke, MCAO surgery or photothrombosis (PT) by cold light illumination was performed to induce focal cerebral ischemia. Six hours after ischemia, mice were administered with TAT-R1D, TAT-s-R1D, or vehicle. The brain infarct was measured 3 days later with TTC staining. We found that TAT-R1D at a single dose of 2 mg/kg bodyweight (i.v.) sufficiently decreased the cerebral infarction compared with mice treated with TAT-s-R1D or vehicle (Fig. 6G and Supplementary Fig. S5C). Furthermore, TAT-R1D treatment markedly improved the overall behavioral functions including neurological score (N.S.) (Supplementary Fig. S5D), Morris water maze (Supplementary Fig. S5E), and open-field test (Supplementary Fig. S5F) analyzed 7 days post-ischemia. Together, our data demonstrate that blockade of DAPK1-Tau interaction by TAT-R1D administration may be a promising target for stroke treatment.

Discussion

Stroke is one of the leading causes of disability and mortality; however, effective measures to minimize brain damage and improve recovery are still lacking. Evidence from a number of studies suggests that spine damage is a preceding neuropathological process contributing to neuronal injury after stroke. This drives us to search for new targets for neuroprotection in the earlier stage of stroke. In the present study, we provide the first evidence that DAPK1-Tau interaction mediates spine damage and neuronal death in cerebral ischemic stroke. Our work also uncovers specific Tau-directed kinase DAPK1, which causes spine damage by phosphorylating Tau at Ser-262 (*p*S262) in the brain with ischemic insults. More importantly, treatment with TAT-R1D (IGSTENLK) results in effective dissociation of DAPK1-Tau

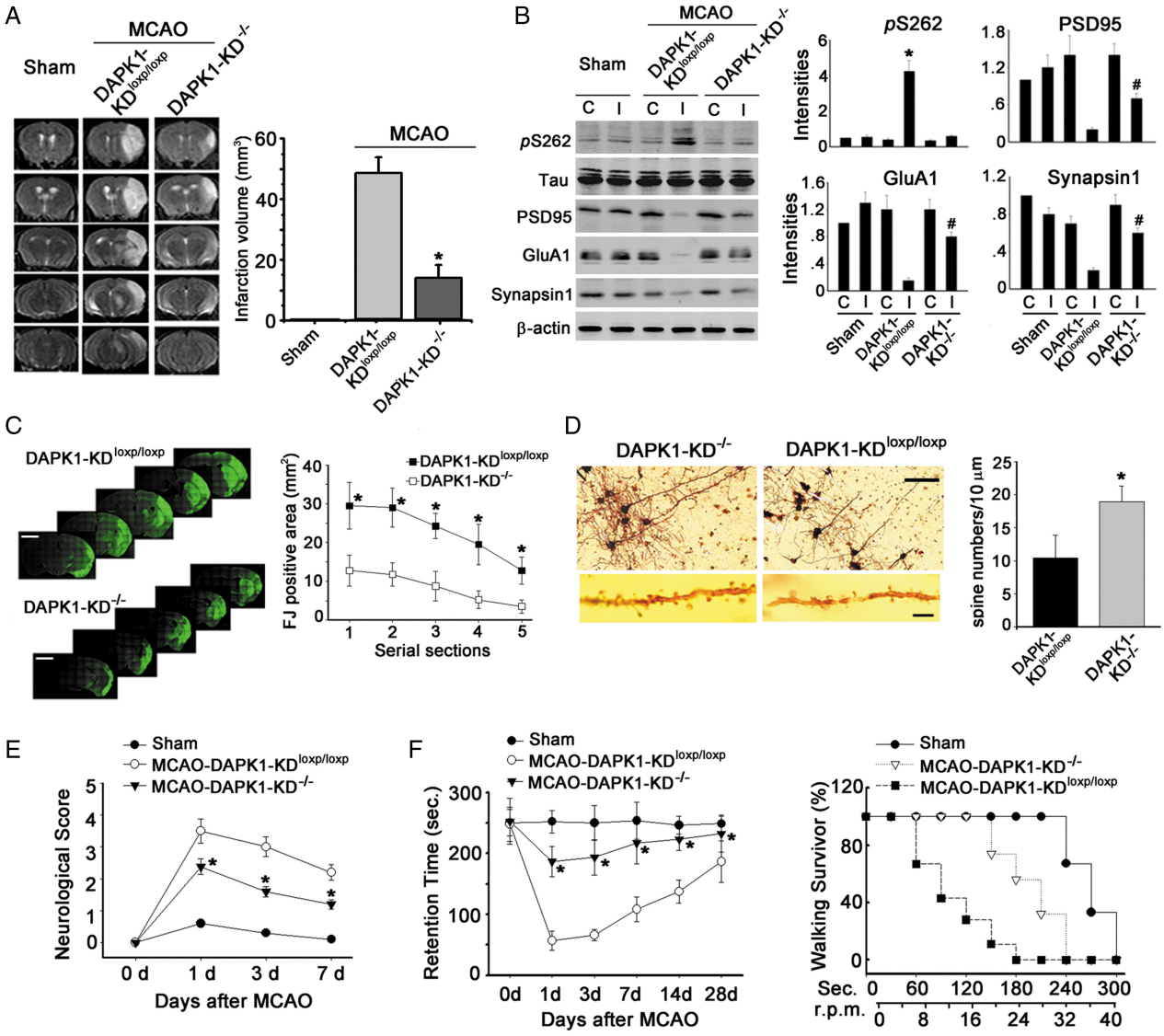

Figure 5. Genetic deletion of DAPK1-KD protects against stroke damage. (*A*) Representative MR images show the area sizes of cerebral infarct. Bar graph shows the quantification of infarct volumes ($n = 5$ for DAPK1-KD$^{-/-}$ mice; $n = 7$ for DAPK1-KD$^{loxp/loxp}$ mice).*$P < 0.05$ vs. DAPK1-KD$^{loxp/loxp}$ mice. (*B*) Immunoblots of the extracts from the ischemic DAPK1-KD$^{-/-}$ and DAPK1-KD$^{loxp/loxp}$ mice cortex probed with *p*S262, Tau, PSD95, GluA1, and Synapsin 1 antibodies. Bar graph shows the quantification of the protein levels ($n = 5$ mice). *$P < 0.05$ vs. DAPK1-KD$^{-/-}$ mice, #$P < 0.05$ vs. DAPK1-KD$^{loxp/loxp}$ mice. (*C*) Representative images show the FJ-labeling in the cortex and striatum. Scale bar in serial pictures is 2.5 mm. Curve lines summarize the FJ-labeled area ($n = 4$). *$P < 0.05$ vs. DAPK1-KD$^{loxp/loxp}$ mice. (*D*) Golgi staining indicated the dendrites in the cortex and numbers of spines (bar graph) in DAPK1-KD$^{-/-}$ and DAPK1-KD$^{loxp/loxp}$ mice 24 h after MCAO ($n = 5$ mice). Scale bar: 100 μm in the upper panel, 10 μm in the lower panel. *$P < 0.05$ vs. DAPK1-KD$^{loxp/loxp}$ mice. (*E*) Overall neurological scores (N.S.) and (*F*) the performance on rotarod test were analyzed throughout the indicated period after MCAO-treated DAPK1-KD$^{-/-}$ and DAPK1-KD$^{loxp/loxp}$ mice. *$P < 0.05$ vs. DAPK1-KD$^{loxp/loxp}$ mice. Data are presented as mean ± SEM.

complexes, causing a significantly decrease in the level of *p*S262, and apparent alleviation of infarction area as well as the neurological deficits induced by cerebral ischemic stroke. Thus, blocking DAPK1-Tau interaction could be a promising target for developing potential therapy for ischemic stroke.

Spine loss is prior to neuronal loss in many neurodegenerative diseases, such as Alzheimer's Diseases, Parkinson Disease. Failure of synaptic transmission can be observed within minutes following hypoxia (Corcoran and O'Connor 2013). Our results are consistent with the previous report that spine damage is a preceding neuropathological process contributing to neuronal injury after stroke, possibly due to the high sensitivity of synaptic activity to alterations in energy supply (Khatri and Man 2013). For example, results from magnetic resonance spectroscopy related the changes in neuroenergetics revealed that more energy were required for functional activation to neurotransmitter cycling at the level of the synapse (Waldvogel et al. 2000; Foo et al. 2012). And the structural and functional integrity of synaptic transmission profoundly depends on a superior oxygen and glucose supply (Acker and Acker 2004).

Tau alteration, dysfunction, and extensive neuron loss have long been associated with several neurodegenerative diseases (Brandt et al. 2005). Abnormal phosphorylation of tau is considered one of the earliest signs of neuronal degeneration and appears to precede tau aggregation (Braak et al. 1994). Site-specific phosphorylation of tau can be regulated by concerted and sequential action of many protein kinases (Stoothoff and Johnson 2005). Among these protein kinases, glycogen synthase kinase-3beta (GSK-3β) was the most powerful tau protein kinase (Jope and Johnson 2004), which could induce the phosphorylation of

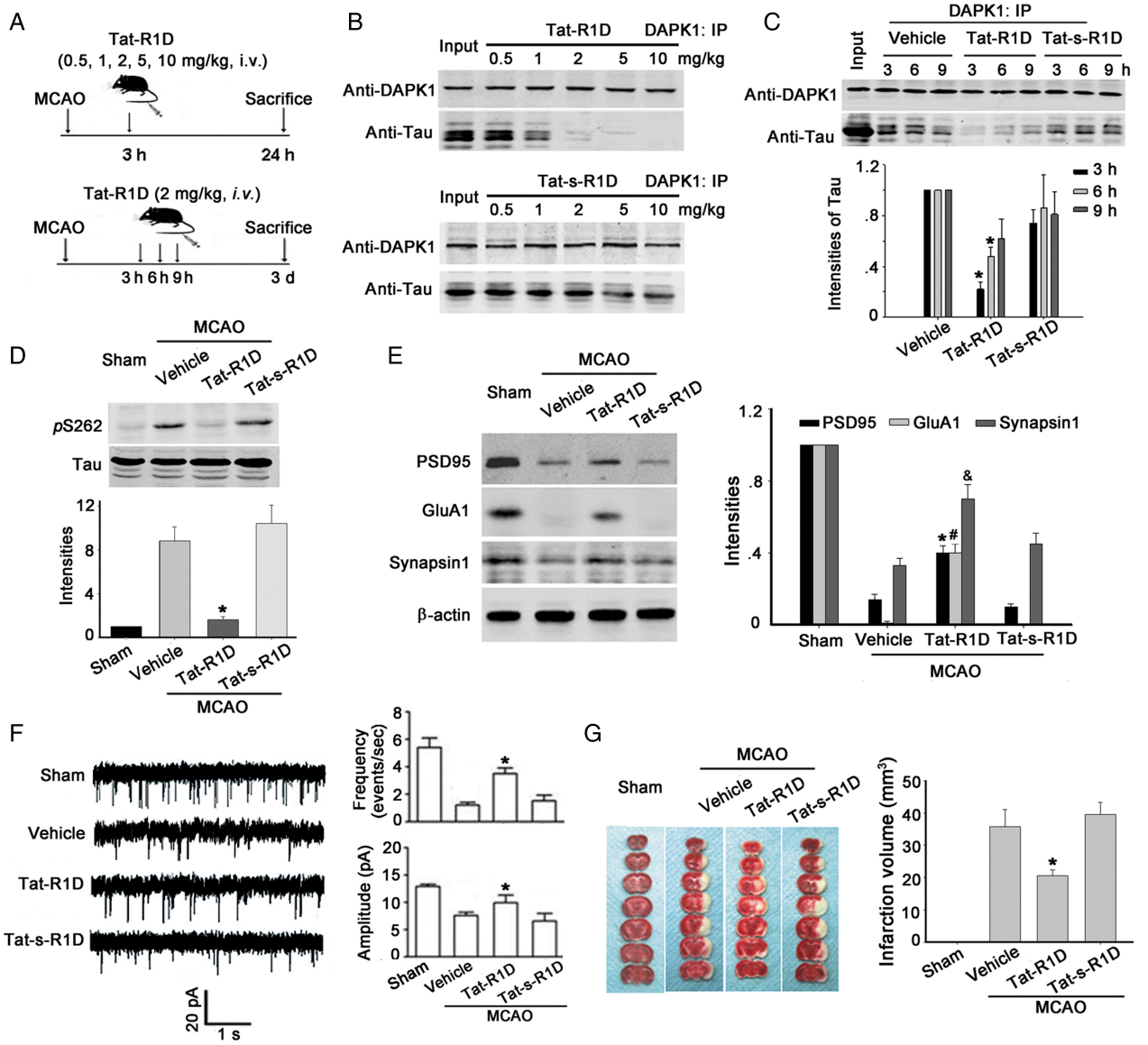

Figure 6. TAT-R1D produces protective effects against spine damage. (*A*) Illustration shows the experimental scheme. (*B*) Representative blots from IP experiments show the dose–response effects of TAT-R1D on DAPK1-Tau association. (*C*) Representative blots and statistical graph show the time-course of TAT-R1D action in an inhibition of DAPK1-Tau association; the cortical extracts (500 μg proteins) administered (i.v.) with TAT-R1D were prepared and precipitated with anti-DAPK1 and blotted with anti-Tau and anti-DAPK1 antibodies 3, 6, or 9 h after MCAO. Input: 20 μg of protein of the extracts without IP was loaded. $^{*}P < 0.05$ vs. vehicle. (*D*) and (*E*) Immunoblots of the extracts from the ischemic mice cortex administered (i.v.) with TAT-R1D 6 h after MCAO probed with anti-*p*S262 antibody (*D*) and PSD95, GluA1 and Synapsin 1 antibodies (*E*). Quantification of the protein levels, band intensities were normalized to the vehicle group ($n = 5$ mice). $^{*}P < 0.05$ (PSD95), $^{\#}P < 0.05$ (GluA1) and $^{\&}P < 0.05$ (Synapsin 1) vs. vehicle. (*F*) Sample traces of mEPSCs recorded at −70 mV in the cortical neurons from TAT-R1D, TAT-s-R1D, or vehicle-treated MCAO mice. Summary graphs from 8 mice sets of normalized mEPSCs frequency and amplitude are shown beneath the traces. $^{*}P < 0.05$ vs. vehicle. (*G*) Representative images of TTC staining show administration of Tat-R1D protects against stroke damage. Bar graph shows the sizes of cerebral infract ($n = 6$ mice). $^{*}P < 0.05$ vs. vehicle. Data are presented as mean ± SEM.

tau protein at many sites, such as Ser199/202 (Leroy et al. 2002). Transient cerebral ischemia could induce the site-specific hyperphosphorylation of tau protein (Wen et al. 2004). Indeed, we only observed the phosphorylation of Ser262, but not Ser199/202 or other previously reported phosphorylation sites (pS202, pS214, pT231, and pS422), indicating the specificity of activation by DAPK1 in cortex after stroke. Changes in tau phosphorylation sites during cerebral ischemia and reperfusion are likely due to changes in the activities of specific phosphatases and kinases (Mailliot et al. 2000). In response to ischemia/reperfusion processes, phosphorylation or dephosphophrylation of tau protein appears to be dynamically regulated at different time phases (Burkhart et al. 1998; Mailliot et al. 2000). Additional studies including high-throughput mass spectrum analysis of phophorylated tau in the different areas of brain or at different time points after stroke, as well as detection of phosphatases or kinases enzyme activity are needed to deepen our understanding of the molecular mechanisms.

We provide several pieces of evidence supporting a causative role of Tau phosphorylation in mediating dendritic spine injuries in ischemic stroke. The phosphorylation of tau at Ser262 may result in the reduction of its affinity to microtubule protein and promote microtubule depolymerization (Biernat et al. 1993), which will inhibit axonal transport, destabilize neuronal

cytoskeleton, and may contribute to the apoptotic process induced by this ischemia/reperfusion insult. In addition, abnormally phosphorylated tau protein is less likely to be hydrolyzed by the proteolylic enzymes and slow in degradation (Gong et al. 2000), resulting in the accumulation in the neurons and the possible formation of indissolvable tau. Those are the possible causes of the increasing of tau in dentritic spines and damage of synapes during ischemia/reperfusion. Taken together, these results demonstrate that tau protein is involved in the pathophysiological mechanism of cerebral ischemia, and therefore interrupting tau phosphorylation may become the target for the treatment of cerebral ischemia.

During ischemic stroke, DAPK1 is activated in the postsynaptic area and phosphorylates NMDA receptor NR2B protein at Serine-1303 and finally contributes to neuronal death (Tu et al. 2010). Our results show the DAPK1-mediated Tau phosphorylation is dependent on its KD and show a different mechanism with DAPK1-p53 interaction, in which DAPK1 associates with p53 DNA-binding motif with its DD and is dependent on the activity of DAPK1. Furthermore, DAPK1-p53-induced cell death is caused by converging the mitochondrial-dependent necrosis pathway and transcriptional-dependent apoptosis pathway (Pei et al. 2014). Whereas DAPK1-Tau-mediated cell death is mainly through the toxicity of phosphorylated tau and its subsequent damage to spines and synapses. Due to the distinct cell death mechanisms of DAPK1-p53 and DAPK1-Tau interaction, we speculate that Tau or p53 is likely to be the different downstream signal of DAPK1 and mediate respective cell death signals. Whether this is a consequence of DAPK1-dependent potentiation of NR2B-containing NMDARs or direct activation of the neuronal death signaling cascade remains to be investigated.

We found that blocking the interaction between DAPK1 and tau by TAT-R1D significantly reduced stroke-induced spine damage and neuronal injury. Furthermore, the transduction of TAT-R1D in the brain tissues occurred rapidly at 3 h after peptide injection and can produce treatment effects up to 6 h after stroke. The therapeutic time window for most neuroprotective agents in stroke is often <4 h following the onset of stroke. Since the blood brain barrier (BBB) often remains intact during the 4-h therapeutic window, any neuroprotective agent that is developed for stroke therapy must be able to cross the intact BBB if administered systemically (Joliot and Prochiantz 2004). In addition, targeted delivery remains a challenge with regard to the application of this technology because TAT fusion proteins administered systemically might also be distributed to other organs, such as liver, kidney, spleen, lung, bowel, and heart, which might cause unexpected side effects (Kilic et al. 2006). Fortunately, it has been found that the distribution of the TAT-RID in many organs has no apparent side effects in the mice (data not shown). Therefore, the fusion peptide TAT-R1D may be a promising agent for future research in stroke with potential clinical application.

In conclusion, our results demonstrate that phosphorylation of Tau at Serine 262 by the KD of DAPK1 mediates spine damage and the subsequent neuronal death in ischemic stroke. Blocking the interaction between DAPK1 and Tau by small peptide of Tau (IGSTENLK) reduces the level of *p*S262 and prevents spine damage and the followed ischemic brain injury. Thus, preventing the DAPK1-Tau pathway by Tat-R1D could be a potential strategy for treating cerebral ischemic stroke.

Supplementary Material

Supplementary material can be found at: http://www.cercor.oxfordjournals.org.

Funding

This work was supported by National Natural Science Foundation of China (Grants: 81130079 and 91232302 to Y.M.L.; 81271270 to Y.S.; 81200863 to L.P.) and China Postdoctoral Science Foundation (2013M540583 to L.P.). Funding to pay the Open Access publication charges for this article was provided by National Natural Science Foundation of China (81130079 and 91232302 to Y.M.L.).

Notes

We greatly appreciate Prof. Hengye Man from Boston University for revising our manuscript; Dr Yihao Yao and Dr Shun Zhang from Radiation Center of Tongji Hospital for the MRI assistance; and Prof. Ruey-Hwa Chen from Institute of Biological Chemistry, Academia Sinica (Taiwan) for presenting the truncated DAPK1 constructs. *Conflict of interest:* None declared.

References

Acker T, Acker H. 2004. Cellular oxygen sensing need in CNS function: physiological and pathological implications. J Exp Biol. 207:3171–3188.

Bialik S, Kimchi A. 2006. The death-associated protein kinases: structure, function, and beyond. Annu Rev Biochem. 75:189–210.

Biernat J, Gustke N, Drewes G, Mandelkow EM, Mandelkow E. 1993. Phosphorylation of Ser262 strongly reduces binding of tau to microtubules: distinction between PHF-like immunoreactivity and microtubule binding. Neuron. 11:153–163.

Braak H, Braak E, Strothjohann M. 1994. Abnormally phosphorylated tau protein related to the formation of neurofibrillary tangles and neuropil threads in the cerebral cortex of sheep and goat. Neurosci Lett. 171:1–4.

Brandt R, Hundelt M, Shahani N. 2005. Tau alteration and neuronal degeneration in tauopathies: mechanisms and models. Biochim Biophys Acta. 1739:331–354.

Burkhart KK, Beard DC, Lehman RA, Billingsley ML. 1998. Alterations in tau phosphorylation in rat and human neocortical brain slices following hypoxia and glucose deprivation. Exp Neurol. 154:464–472.

Chen L, Jiang M, Pei L. 2012. Comparison of three methods of drug delivery in the rat lumbar spinal subarachnoid space. Anat Rec (Hoboken). 295:1212–1220.

Corcoran A, O'Connor JJ. 2013. Hypoxia-inducible factor signalling mechanisms in the central nervous system. Acta Physiol (Oxf) 208:298–310.

Foo K, Blumenthal L, Man HY. 2012. Regulation of neuronal bioenergy homeostasis by glutamate. Neurochem Int. 61:389–396.

Gong CX, Lidsky T, Wegiel J, Zuck L, Grundke-Iqbal I, Iqbal K. 2000. Phosphorylation of microtubule-associated protein tau is regulated by protein phosphatase 2A in mammalian brain. Implications for neurofibrillary degeneration in Alzheimer's disease. J Biol Chem. 275:5535–5544.

Hofmeijer J, van Putten MJ. 2012. Ischemic cerebral damage: an appraisal of synaptic failure. Stroke. 43:607–615.

Ittner LM, Ke YD, Delerue F, Bi M, Gladbach A, van Eersel J, Wolfing H, Chieng BC, Christie MJ, Napier IA et al. 2010. Dendritic function of tau mediates amyloid-beta toxicity in Alzheimer's disease mouse models. Cell. 142:387–397.

Joliot A, Prochiantz A. 2004. Transduction peptides: from technology to physiology. Nat Cell Biol. 6:189–196.

Jope RS, Johnson GV. 2004. The glamour and gloom of glycogen synthase kinase-3. Trends Biochem Sci. 29:95–102.

Khatri N, Man HY. 2013. Synaptic activity and bioenergy homeostasis: implications in brain trauma and neurodegenerative diseases. Front Neurol. 4:199.

Kilic E, Kilic U, Hermann DM. 2006. TAT fusion proteins against ischemic stroke: current status and future perspectives. Front Biosci. 11:1716–1721.

Lee VM, Goedert M, Trojanowski JQ. 2001. Neurodegenerative tauopathies. Annu Rev Neurosci. 24:1121–1159.

Leroy K, Boutajangout A, Authelet M, Woodgett JR, Anderton BH, Brion JP. 2002. The active form of glycogen synthase kinase-3beta is associated with granulovacuolar degeneration in neurons in Alzheimer's disease. Acta Neuropathol. 103: 91–99.

Mailliot C, Podevin-Dimster V, Rosenthal RE, Sergeant N, Delacourte A, Fiskum G, Buee L. 2000. Rapid tau protein dephosphorylation and differential rephosphorylation during cardiac arrest-induced cerebral ischemia and reperfusion. J Cereb Blood Flow Metab. 20:543–549.

Morris M, Maeda S, Vossel K, Mucke L. 2011. The many faces of tau. Neuron. 70:410–426.

Paxinos G, Franklin K. 2012. Paxinos and Franklin's the mouse brain in stereotaxic coordinates. Salt Lake City (UT): American Academic Press.

Pei L, Shang Y, Jin H, Wang S, Wei N, Yan H, Wu Y, Yao C, Wang X, Zhu LQ et al. 2014. DAPK1-p53 interaction converges necrotic and apoptotic pathways of ischemic neuronal death. J Neurosci. 34:6546–6556.

Pei L, Zhang J, Zhao F, Su T, Wei H, Tian J, Li M, Shi J. 2011. Annexin 1 exerts anti-nociceptive effects after peripheral inflammatory pain through formyl-peptide-receptor-like 1 in rat dorsal root ganglion. Br J Anaesth. 107:948–958.

Stoothoff WH, Johnson GV. 2005. Tau phosphorylation: physiological and pathological consequences. Biochim Biophys Acta. 1739:280–297.

Tu W, Xu X, Peng L, Zhong X, Zhang W, Soundarapandian MM, Balel C, Wang M, Jia N, Zhang W et al. 2010. DAPK1 interaction with NMDA receptor NR2B subunits mediates brain damage in stroke. Cell. 140:222–234.

Waldvogel D, van Gelderen P, Muellbacher W, Ziemann U, Immisch I, Hallett M. 2000. The relative metabolic demand of inhibition and excitation. Nature. 406:995–998.

Wang X, Pei L, Yan H, Wang Z, Wei N, Wang S, Yang X, Tian Q, Lu Y. 2014. Intervention of death-associated protein kinase 1-p53 interaction exerts the therapeutic effects against stroke. Stroke. 45:3089–3091.

Wen Y, Yang S, Liu R, Simpkins JW. 2004. Transient cerebral ischemia induces site-specific hyperphosphorylation of tau protein. Brain Res. 1022:30–38.

Xue Y, Ren J, Gao X, Jin C, Wen L, Yao X. 2008. GPS 2.0, a tool to predict kinase-specific phosphorylation sites in hierarchy. Mol Cell Proteomics. 7:1598–1608.

Yang Y, Shu X, Liu D, Shang Y, Wu Y, Pei L, Xu X, Tian Q, Zhang J, Qian K et al. 2012. EPAC null mutation impairs learning and social interactions via aberrant regulation of miR-124 and Zif268 translation. Neuron. 73:774–788.

Zheng GQ, Wang XM, Wang Y, Wang XT. 2010. Tau as a potential novel therapeutic target in ischemic stroke. J Cell Biochem. 109:26–29.